

Diff4MMLiTS: Advanced Multimodal Liver Tumor Segmentation via Diffusion-Based Image Synthesis and Alignment

Shiyun Chen^{1†}, Li Lin^{1,2†}, Pujin Cheng^{1,2}, ZhiCheng Jin³, JianJian Chen³, HaiDong Zhu³,
Kenneth K. Y. Wong², Xiaoying Tang^{1,4,*}

¹Department of Electronic and Electrical Engineering, Southern University of Science and Technology, Shenzhen, China

²Department of Electrical and Electronic Engineering, The University of Hong Kong, Hong Kong SAR, China

³Center of Interventional Radiology and Vascular Surgery, Nurturing Center of Jiangsu Province for State Laboratory of AI Imaging & Interventional Radiology (Southeast University), Department of Radiology, Zhongda Hospital, Medical School, Southeast University, Nanjing, China

⁴Jiaxing Research Institute, Southern University of Science and Technology, Jiaxing, China

Abstract—Multimodal learning has been demonstrated to enhance performance across various clinical tasks, owing to the diverse perspectives offered by different modalities of data. However, existing multimodal segmentation methods rely on well-registered multimodal data, which is unrealistic for real-world clinical images, particularly for indistinct and diffuse regions such as liver tumors. In this paper, we introduce Diff4MMLiTS, a four-stage multimodal liver tumor segmentation pipeline: pre-registration of the target organs in multimodal CTs; dilation of the annotated modality’s mask and followed by its use in inpainting to obtain multimodal normal CTs without tumors; synthesis of strictly aligned multimodal CTs with tumors using the latent diffusion model based on multimodal CT features and randomly generated tumor masks; and finally, training the segmentation model, thus eliminating the need for strictly aligned multimodal data. Extensive experiments on public and internal datasets demonstrate the superiority of Diff4MMLiTS over other state-of-the-art multimodal segmentation methods.

Index Terms—Multimodal Learning, Liver Tumor Segmentation, Diffusion-Based Synthesis

I. INTRODUCTION

Liver tumor segmentation is crucial for clinical diagnosis and treatment. Previous studies have achieved notable results in unimodal liver tumor segmentation, confirming the effectiveness of deep learning techniques in this area [1], [2]. As different types of tumors exhibit distinct characteristics across various modalities, clinical radiologists often use multimodal

CTs for more comprehensive diagnosis and more precise delineation of tumor boundaries [3]. Integrating multimodal information significantly enhances segmentation performance [4], [5]. However, compared to unimodal, the high annotation costs, privacy concerns, and data scarcity significantly constrain the exploration of multimodal segmentation methods.

Recent multimodal learning studies have underscored the importance of data alignment [6]–[8]. Alignment is equally vital in multimodal medical image segmentation tasks. Public multimodal benchmarks like BraTS [9] and AutoPET [10] either employ standardized anatomical templates for rigid alignment or are collected simultaneously, inherently ensuring rigid data alignment. Thus, most current multimodal tumor segmentation methods operate under the assumption of strict data alignment, focusing primarily on multimodal fusion methods [11], [12]. In contrast, in real clinical settings, multimodal CT images often exhibit incomplete alignment or significant misalignment due to the spatiotemporal differences in data acquisition. Although some registration methods based on traditional paradigms (e.g., differential homogeneous deformation [13]) or deep learning [14], [15] have been proposed and achieved reasonable registration at the organ or tissue level, they still struggle to fully align the diffuse and indistinct tumor regions. This presents unavoidable noise for existing multimodal segmentation algorithms.

Concurrently, due to the limited availability of images with tumors and the rising popularity of generative AI, recent studies have employed generative models (such as those based on Generative Adversarial Networks (GANs) or diffusion models to synthesize liver tumors [16], [17], demonstrating potential in enhancing tumor segmentation performance. However, these methods are confined to unimodal segmentation tasks and require normal CTs (without tumors) as synthesis conditions,

This study was supported by the National Key Research and Development Program of China (2023YFC2415400); the National Natural Science Foundation of China (T2422012, 62071210); the Guangdong Basic and Applied Basic Research (2024B1515020088); the Shenzhen Science and Technology Program (RCYX20210609103056042); the Guangdong Basic and Applied Basic Research (2021A1515220131); the High Level of Special Funds (G030230001, G03034K003).

[†]These authors contributed equally.

*Corresponding author: Dr. Xiaoying Tang (tangxy@sustech.edu.cn)

somewhat restricting their application. Nevertheless, these synthetic tumor efforts provide two key insights: first, diverse tumor samples can be synthesized to alleviate the challenge of data scarcity and to enhance model generalization; second, synthesizing rigorously aligned multimodal CTs can partially mitigate the current dependence of segmentation algorithms on well-registered multimodal data.

In such a context, we present an innovative and effective multimodal segmentation framework named Diff4MMLiTS. Specifically, the process begins with preliminary registration and data preprocessing, during which the target organ is roughly aligned, but the tumor remains misaligned. Therefore, we employ the mask of the annotated modality, dilating it to ensure adequate coverage of the tumor across various modalities. Subsequently, this mask is utilized in the Normal CT Generator (NCG) module for inpainting, yielding the normal CT. Within the latent space, the Multimodal CT Synthesizer (MCS) module leverages the multimodal CT features and randomly generated tumor masks to synthesize strictly aligned multimodal CTs with tumors. The aforementioned synthesis process employs the common mask, yet each modality’s CT is synthesized according to its unique feature distribution mapping. Finally, the roughly aligned real data is combined with the fully aligned synthetic data to train the segmentation model. Our contributions are as follows:

- An innovative multimodal segmentation framework, Diff4MMLiTS, is proposed to be the first multimodal tumor segmentation framework based on diffusion synthesis as far as we know.
- The Inpainting-Synthesis-Segmentation pipeline is designed to innovatively translate the challenges of tumor registration into a data synthesis problem, and the framework can be adapted to a variety of multimodal datasets without the need for perfect alignment.
- Diff4MMLiTS is assessed on both internal and external datasets, with experimental results demonstrating that our method significantly surpasses existing multimodal segmentation techniques. Code and synthetic dataset will be available.

II. RELATED WORK

Multimodal segmentation aims to integrate information from different modalities through methods such as input fusion [2], feature interaction [12], and output fusion [4] to achieve better segmentation performance. For instance, mmformer [18] and RFNet [19] employ the transformer and CNN, respectively, to learn features across different modalities of brain tumors. However, common multimodal segmentation methods assume that the source images are strictly aligned at the pixel level. In contrast, in real clinical practice, multimodal images are often acquired at different times and using different imaging devices. Even with registration, perfect alignment is difficult to achieve, especially when dealing with localized lesions. To address this issue, researchers have developed novel methods for unregistered multimodal images, such as

PAMRFuse [20] and Bsafusion [21]; however, these primarily focus on cross-modal fusion rather than multimodal segmentation. Our framework focuses on multimodal liver tumor segmentation, enhancing segmentation performance by addressing the alignment issue.

Medical image synthesis is also a highly regarded research topic, commonly applied in tasks such as missing modality completion, data augmentation, and data-efficient learning. Existing medical image synthesis methods are primarily based on GANs [22] and diffusion models [23], [24]. Some studies also explore tumor synthesis, such as Red-GAN [25] and LF-SynthSeg [26], focusing on synthesizing multimodal brain tumors. However, these methods are not specifically designed for liver tumor synthesis. Chen et al. [16] propose a diffusion-based method that successfully generates abdominal tumors. Wu et al. [17] introduce an adversarial training strategy that leverages unlabeled data for synthetic training. Although these methods are designed for liver tumors, they are constrained to unimodal synthesis and fail to exhibit the anticipated advantages when directly applied to multimodal tasks. To address these issues, we propose a synthetic image-based multimodal liver tumor segmentation framework that effectively tackles alignment issues in multimodal segmentation tasks by generating perfectly aligned multimodal data.

III. METHOD

Diff4MMLiTS comprises three pivotal components: the Normal CT Generator (NCG) module, the Multimodal CT Synthesizer (MCS) module, the Multimodal Segmenter (MS) module. These components are trained sequentially, with each preceding stage’s output serving as input for the next. The NCG module provides the CT background for the MCS module to synthesize CT images with tumor. The MCS module then supplies the MS module with synthetic images to train the segmenter. The following subsections will provide a detailed elaboration. The overall framework is shown in Fig. 1.

A. Normal CT Generator (NCG) Module

Since there is no publicly available paired multimodal normal CT dataset, the NCG module is used to generate paired multimodal normal CT data as the basis for tumor data synthesis. Inpainting involves reconstructing the missing or masked regions of an image [27]. Inspired by Suvorov [28], we employ an inpainting network based on Fast Fourier Convolution (FFC), which enhances the receptive field, ultimately achieving large mask inpainting with an image-wide receptive field. To reduce computational load, we perform slice-by-slice inpainting of 2D slices within 3D CT scans.

Given an image $x \in \mathbb{R}^{H \times W \times 3}$ and a binary mask of the inpainting regions $m \in \mathbb{R}^{H \times W \times 1}$, stacking them will give: $x' = \text{stack}(x \odot m, m)$, where $x \odot m$ denotes the masked image. The feed-forward inpainting network $f_{\theta}(\cdot)$ then processes the input x' in a fully convolutional manner, then generates the inpainted image: $\hat{x} = f_{\theta}(x')$. Specifically, the image and mask pair serve as network inputs, which are downsampled into FFC residual blocks. During FFC processing, the input is divided

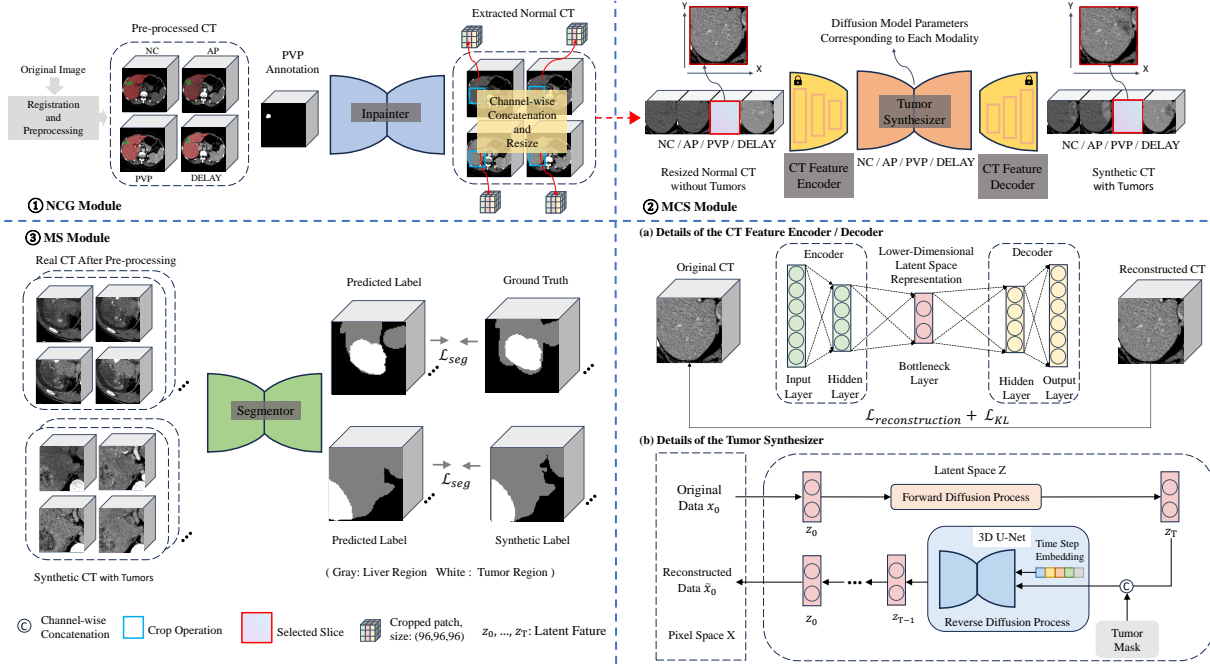


Fig. 1. The architecture of Diff4MMLiTS. Normal CT Generator (NCG) module uses the extended PVP mask to inpaint multimodal images to acquire normal CTs. Multimodal CT Synthesizer (MCS) module uses normal CTs to synthesize multimodal CTs. Multimodal Segmenter (MS) module trains segmenter using real and synthetic data. MCS comprises two components: a 3D autoencoder consisting of a CT feature encoder and decoder, a tumor synthesizer based on a diffusion model (DM).

into two parallel branches: a local branch, using traditional convolution, captures local information, while a global branch, based on real FFT, acquires global contextual information. These two outputs are then cross-fused and channel-wise concatenated to produce the final output.

We fine-tune the model using pre-trained parameters and followed the training strategy of Suvorov et al [28]. For the fine-tuning of NCG, we employ original internal multimodal data to adapt it to the inpainting of multimodal CT images. After training, the inpainter is utilized to remove tumor foreground regions from multimodal CT with tumors. For each tumor region in the portal venous phase (PVP) mask, a 5×5 kernel is first employed for morphological closing, followed by a single iteration of dilation using a 3×3 kernel, to mitigate subjective noise and ensure maximal coverage of tumor regions across all modalities. NCG used the dilated PVP noise annotation as the mask to remove the foreground from labeled samples, ultimately producing a corresponding normal CT for each multimodal CT.

B. Multimodal CT Synthesizer (MCS) Module

Recently, diffusion models have achieved remarkable success in the synthesis of medical images. Inspired by Robin Rombach [29], we design a latent feature-based diffusion process capable of synthesizing multimodal liver tumors within latent space, significantly reducing computational complexity while maintaining synthesis quality. MCS is divided into two stages: first, a autoencoder is trained to learn comprehensive latent features, including the CT feature encoder \mathcal{E} and decoder

\mathcal{D} ; second, a tumor synthesizer based on a latent diffusion model (LDM) is trained to generate synthetic images.

Specifically, the VQGAN-based autoencoder performs the encoding and reconstruction between the image x_0 and its latent representation z_0 , giving $\tilde{x}_0 = \mathcal{D}(z_0) = \mathcal{D}(\mathcal{E}(x_0))$. Since the universal autoencoding stage only requires training once and can be utilized repeatedly for multiple diffusion model trainings [29], we adapt the pre-trained autoencoder [16]. The diffusion process transpires within the latent space Z , where synthesized image features are reconstructed into the pixel space X .

The diffusion process comprises a forward process and a reverse process. The forward diffusion process transforms the data distribution into a standard Gaussian distribution at each time step $t \in [1, \dots, T]$ by the following process:

$$q(z_t | z_0) = \mathcal{N}(z_t | \sqrt{\bar{\alpha}_t} z_0, (1 - \bar{\alpha}_t) \epsilon), \quad (1)$$

where ϵ is the random noise, $\bar{\alpha}_t$ denotes the noise level.

The reverse generation process aims to gradually generate data samples from the noise by the following process:

$$p(z_0) = p(z_T) \prod_{t=1}^T p(z_{t-1} | z_t, y), \quad (2)$$

where y is the tumor mask for conditioning information. During the inference stage, a coordinate within the liver region is randomly selected as the center point, and random values for the semi-axes x , y , and z are assigned. An ellipsoidal mask approximating the tumor is then generated based on these parameters, followed by elastic deformation to produce

the tumor mask y , indicating the location of the synthesized tumor. During the training stage, $\epsilon_\theta(\cdot)$ denotes the denoising encoder, the training objective of LDM can be written as:

$$\mathcal{L}_{LDM} := \mathbb{E}_{\mathcal{E}(x_0), \epsilon \sim \mathcal{N}(0,1), t} [\|\epsilon - \epsilon_\theta(z_t, y, t)\|_2^2]. \quad (3)$$

C. Multimodal Segmentation (MS) Module

The segmenter is a U-shape network. During training, MS dynamically synthesizes CTs with tumors from inpainted CTs, thereby constructing a hybrid dataset that combines synthetic and real data. The training objective of the segmenter is to minimize the voxel classification error relative to the ground truth. The loss function \mathcal{L}_{seg} is consist of the Dice loss \mathcal{L}_{dice} and the cross-entropy loss \mathcal{L}_{ce} , which can be written as:

$$\mathcal{L}_{seg} = \mathcal{L}_{dice} + \gamma \mathcal{L}_{ce}, \quad (4)$$

where γ is a factor for balancing the two loss contributions.

During inference, if the input does not consist of all four modalities, certain modalities will be duplicated to match the input size required by the model. For example, if only a single modality is present, it will be replicated four times and then concatenated before being fed into the segmentation model.

IV. EXPERIMENTS AND RESULTS

A. Datasets

To the best of our knowledge, there is currently no well-aligned publicly available multimodal liver tumor CT dataset. Therefore, we construct an in-house dataset, mmLiTs, based on multimodal abdominal CT data from Zhongda Hospital, Southeast University. After excluding cases with indistinct boundaries across all CTs, the final dataset includes 45 sets of four-phase abdominal CTs with in-plane resolutions of 512×512 , spacing from 0.6445 mm to 0.9160 mm, slice counts ranging from 45 to 561, and thicknesses between 1.0 mm and 5.0 mm. Experienced radiologists manually annotated liver tumors, and the data are randomly split into training, validation, and test sets in a 3:1:1 ratio. Given that radiologists often use PVP images to identify tumor margins that are less discernible in other phases, the dataset provides annotations for PVP and attempts to register other modalities to PVP.

Additionally, we assess the generalizability of our method on the LiTS dataset [30]. Since the LiTS dataset is a unimodal dataset and does not involve multimodal alignment issues, we directly stack its unimodal images four times to match the input requirement of the segmentation model. We apply the same processing to all comparison methods, including Diff4MMLiTS, to ensure a fair performance comparison.

B. Implementation Details

Diff4MMLiTS is implemented by PyTorch on a workstation equipped with NVIDIA RTX 3090. We use nnUNet as the default backbone. To avoid over-fitting, online data augmentations, including random flipping, rotation, and color jittering, are applied. All methods are trained for 1000 epochs. The preprocessing involves clipping the images to a $[-21, 189]$ window and normalizing them to zero mean and unit standard

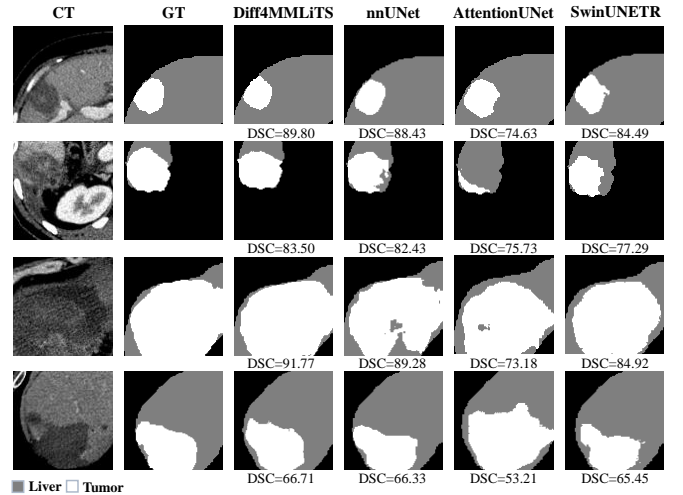


Fig. 2. Qualitative visualization results.

TABLE I
QUANTITATIVE COMPARISONS OF DIFF4MMLiTS WITH SOTA METHODS ON MMLiTS. THE BEST RESULTS ARE HIGHLIGHTED IN BOLD.

Methods	DSC(%)	JAC(%)	SE(%)	PRE(%)
16'U-Net [1]	75.46	61.29	68.12	87.69
16'V-Net [31]	75.97	62.70	81.78	74.40
18'AttentionUNet [32]	67.80	53.75	65.25	77.72
18'mUNet [2]	76.34	62.77	69.84	86.47
22'SwinUNETR [33]	77.28	63.41	71.72	86.02
18'SegResNet [34]	77.73	64.05	75.29	81.87
21'MAML [4]	76.06	63.08	67.92	91.27
22'mmformer [18]	77.32	64.32	78.76	77.94
23'A2FSeg [12]	69.74	55.90	61.93	88.66
24'PA-Net [5]	76.56	63.09	74.38	82.23
Diff4MMLiTS	79.02	66.33	74.47	85.24

deviation, followed by random cropping of $96 \times 96 \times 96$ patches as input. The postprocessing filters the detection results by retaining only tumors located within the liver region. For the loss function, we set the value of γ to 0.5.

The Dice Similarity Coefficient (DSC), Jaccard index (JAC), Sensitivity (SE), and Precision (PRE) are used to quantitatively evaluate the performance of Diff4MMLiTS and other state-of-the-art (SOTA) methods.

C. Overall Performance

To evaluate our method, we compare Diff4MMLiTS with various general and multimodal segmentation methods. Given that achieving precise liver segmentation is relatively straightforward, we focus specifically on the segmentation of intra-hepatic tumors. The comparison results are presented in Table I, with visualizations shown in Fig. 2.

Compared to the U-Net and its variants, our method enhances the DSC by 1.74% over the second-best SwinUNETR. When compared with other multimodal medical image segmentation models, our method enhances DSC by 1.29% over

TABLE II
COMPARISON OF EXPERIMENTAL RESULTS ON LiTS. THE BEST RESULTS ARE HIGHLIGHTED IN BOLD.

Methods	DSC(%)	JAC(%)	SE(%)	PRE(%)
nnUNet (real tumors)	41.63	27.37	55.51	35.56
Diff4MMLiTS	57.75	42.99	59.41	64.59

TABLE III
RESULTS OF DIFF4MMLiTS EQUIPPED WITH DIFFERENT BACKBONE MODELS. THE BEST RESULTS ARE HIGHLIGHTED IN BOLD.

Methods	DSC(%)	JAC(%)	SE(%)	PRE(%)
U-Net [1]	75.46	61.29	68.12	87.69
U-Net w/ Diff4MMLiTS	77.41	64.25	72.22	85.17
AttentionUNet [32]	67.80	53.75	65.25	77.72
AttentionUNet w/ Diff4MMLiTS	74.38	60.40	67.37	84.58
nnUNet [2]	76.34	62.77	69.84	86.47
nnUNet w/ Diff4MMLiTS	79.02	66.33	74.47	85.24

the second best SegResNet. Moreover, Diff4MMLiTS significantly reduces false positives and false negatives, as reflected in the improved SE and PRE. This indicates enhanced tumor detection capability and a diminished likelihood of missed or incorrect detections. Overall, our proposed method has excellent superiority and achieves the best performance in the multimodal liver tumor segmentation task.

D. Generalizability and Adaptability of Diff4MMLiTS

We evaluate the results of our proposed method on publicly available external datasets to verify that the model trained with Diff4MMLiTS can effectively generalize to out-of-distribution data without the need for retraining on the new dataset. All methods are trained on mmLiTs and tested on lesion samples selected from LiTS. The comparison results as shown in Table II. Compared to nnUNet fully trained on real data, Diff4MMLiTS with the synthesis strategy achieves a 16.12% improvement in DSC. This implies that training models with such reliable synthetic images can effectively mitigate the risk of overfitting to in-distribution samples, thereby enhancing their ability to generalize to out-of-distribution samples. This underscores the potential of the proposed method as a promising solution for liver tumor screening.

To further evaluate the adaptability of Diff4MMLiTS, we use three backbone models in the MS module, namely U-Net, AttentionUNet, and nnUNet, with results presented in Table III. The findings indicate that our framework adapts seamlessly to all backbones, achieving notable performance improvements. Compared to segmentation models trained solely on real data, those employing the hybrid training strategy show improvements of 1.95%, 6.58%, and 2.68% in DSC. This identifies the adaptability of our framework to different backbone models and the effectiveness of the hybrid training strategy in enhancing segmentation performance.

TABLE IV
RESULTS USING ONLY A PORTION OF REAL DISEASED CT AND CORRESPONDING NORMAL CT TRAINING. NOTE THAT UNI IS SHORT FOR UNIMODAL AND MULTI IS SHORT FOR MULTIMODAL.

Ratio(diseased/normal)	DSC(%)	JAC(%)	SE(%)	PRE(%)
uni 100% (29/29)	71.24	56.08	64.31	85.11
10% (3/3)	73.87	59.58	76.40	73.13
30% (9/9)	75.26	60.53	70.24	84.14
multi 50% (15/15)	76.97	63.45	70.25	87.43
70% (20/20)	78.49	65.47	75.66	82.47
100% (29/29)	79.02	66.33	74.47	85.24

TABLE V
RESULTS OF DIFF4MMLiTS EQUIPPED WITH DIFFERENT INPAINTING OR SYNTHESIS METHODS. \$ DENOTES THE REPLACEMENT OF THE INPAINTER AND # DENOTES THE REPLACEMENT OF THE DIFFUSION MODEL. THE BEST RESULTS ARE HIGHLIGHTED IN BOLD.

Methods	DSC(%)	JAC(%)	SE(%)	PRE(%)
Median (\$)	74.79	60.75	79.43	73.37
CUT-GAN (#)	77.64	63.92	74.78	84.62
Diff4MMLiTS	79.02	66.33	74.47	85.24

E. Effectiveness of Multimodal Synthesis Strategy

As illustrated in Table IV, we further evaluate the performance of the synthesis strategy on multimodal and unimodal segmentation methods. In all quantity settings, we employ nnUNet as the segmentation model architecture. The performance of unimodal segmentation models typically rely heavily on the quantity and diversity of training data, but our method requires only a small subset of multimodal data to exceed the performance of models trained on fully annotated unimodal data. The results indicate that when employing merely 10% of the data (real samples and inpaint-based normal multimodal CTs from three patients) as the training set for the segmentation model, it yields a DSC that is 2.63% higher than that of unimodal segmentation models. Furthermore, even when compared to multimodal segmentation models, our method achieves comparable results using only 70% of the paired training data. These findings confirm the effectiveness of our Diff4MMLiTS in enhancing the performance of liver tumor segmentation models.

F. Contribution of Different Modules to the Framework

In our framework, each stage is trained independently, with the output of one stage serving as the input for the subsequent one. This sequential training method ensures that each component is optimized for its specific role before integration into the overall framework. To comprehensively validate the importance of each module, we explore alternative methods by replacing the inpainter and the diffusion-based synthesis module. Specifically, we replace the inpainter in NCG with a median filter. On the other hand, we replace the proposed latent diffusion-based MCS module with CUT-GAN

[35], which constructs the domain of images to be transformed by concatenating normal CTs with randomly generated tumor masks, and learns the mapping between this domain and the domain of the CT image with real tumor.

The impact of these alternatives on the overall framework's performance is shown in Table V. The results indicate that the framework with the original inpainter and synthesizer achieves the best performance. Compared to the proposed NCG, the CT images generated by the median filter introduce noise and disrupt the original details, thereby affecting the quality of subsequent tumor synthesis. Additionally, the tumor images synthesized by CUT-GAN are overly smooth, making the complementary features between multimodal tumors less pronounced, which, in turn, affects the performance of the segmentation model. In contrast, the inpainter and synthesizer proposed in our original framework not only preserve background details but also generate diverse and high-quality multimodal liver tumors, playing a crucial role in the liver tumor segmentation task.

V. CONCLUSION

This paper presents a novel multimodal liver tumor segmentation framework, named Diff4MMLiTS. Diff4MMLiTS is a diffusion-based pipeline comprising of a Normal CT Generator, a Multimodal CT Synthesizer and a Multimodal Segmenter. Extensive experiments demonstrate the superiority of our framework. A potential future direction is to employ an all-in-one diffusion model paradigm for multimodal tumor synthesis while exploring advanced network designs and multimodal fusion strategies to further enhance performance.

REFERENCES

- [1] Özgün Çiçek, Ahmed Abdulkadir, Soeren S Lienkamp, Thomas Brox, and Olaf Ronneberger, "3d u-net: learning dense volumetric segmentation from sparse annotation." Springer, 2016, pp. 424–432.
- [2] Fabian Isensee, Paul F Jaeger, Simon AA Kohl, Jens Petersen, and Klaus H Maier-Hein, "nnu-net: a self-configuring method for deep learning-based biomedical image segmentation," *Nature methods*, vol. 18, no. 2, pp. 203–211, 2021.
- [3] Yue Zhang, Chengtao Peng, Ruofeng Tong, Lanfen Lin, Yen-Wei Chen, Qingqing Chen, Hongjie Hu, and S Kevin Zhou, "Multi-modal tumor segmentation with deformable aggregation and uncertain region inpainting," *IEEE Transactions on Medical Imaging*, vol. 42, no. 10, pp. 3091–3103, 2023.
- [4] Yao Zhang, Jiawei Yang, Jiang Tian, Zhongchao Shi, Cheng Zhong, Yang Zhang, and Zhiqiang He, "Modality-aware mutual learning for multi-modal medical image segmentation," in *International Conference on Medical Image Computing and Computer-Assisted Intervention*. Springer, 2021, pp. 589–599.
- [5] Zhenbing Liu, Junfeng Hou, Xipeng Pan, Ruojie Zhang, and Zhenwei Shi, "Pa-net: A phase attention network fusing venous and arterial phase features of ct images for liver tumor segmentation," *Computer Methods and Programs in Biomedicine*, vol. 244, pp. 107997, 2024.
- [6] Pujin Cheng, Li Lin, Junyan Lyu, Yijin Huang, Wenhan Luo, and Xiaoying Tang, "Prior: Prototype representation joint learning from medical images and reports," *International Conference on Computer Vision (ICCV)*, pp. 21304–21314, 2023.
- [7] Jean-Baptiste Alayrac, Jeff Donahue, Pauline Luc, Antoine Miech, Iain Barr, Yana Hasson, et al., "Flamingo: a visual language model for few-shot learning," *ArXiv*, vol. abs/2204.14198, 2022.
- [8] Chunyuan Li, Cliff Wong, Sheng Zhang, Naoto Usuyama, Haotian Liu, Jianwei Yang, et al., "Llava-med: Training a large language-and-vision assistant for biomedicine in one day," *Advances in Neural Information Processing Systems*, vol. 36, 2024.
- [9] Bjoern H Menze, Andras Jakab, Stefan Bauer, Jayashree Kalpathy-Cramer, Keyvan Farahani, Justin Kirby, et al., "The multimodal brain tumor image segmentation benchmark (brats)," *IEEE Transactions on Medical Imaging*, vol. 34, pp. 1993–2024, 2015.
- [10] Sergios Gatidis, Tobias Hepp, Marcel Früh, Christian La Fougère, Konstantin Nikolaou, Christina Pfannenber, et al., "A whole-body fdg-pet/ct dataset with manually annotated tumor lesions," *Scientific Data*, vol. 9, 2022.
- [11] Hengyi Yang, Tao Zhou, Yi Zhou, Yizhe Zhang, and Huazhu Fu, "Flexible fusion network for multi-modal brain tumor segmentation," *IEEE Journal of Biomedical and Health Informatics*, vol. 27, pp. 3349–3359, 2023.
- [12] Zirui Wang and Yi Hong, "A2fseg: Adaptive multi-modal fusion network for medical image segmentation," in *International Conference on Medical Image Computing and Computer-Assisted Intervention*. Springer, 2023, pp. 673–681.
- [13] Mark Jenkinson, Christian F Beckmann, Timothy EJ Behrens, Mark W Woolrich, and Stephen M Smith, "Fsl," *Neuroimage*, vol. 62, no. 2, pp. 782–790, 2012.
- [14] Boah Kim, Dong Hwan Kim, Seong Ho Park, Jieun Kim, June-Goo Lee, and Jong Chul Ye, "Cyclemorph: Cycle consistent unsupervised deformable image registration," *Medical Image Analysis*, vol. 71, pp. 102036, 2020.
- [15] Junyu Chen, Eric C Frey, Yufan He, William P Segars, Ye Li, and Yong Du, "Transmorph: Transformer for unsupervised medical image registration," *Medical Image Analysis*, vol. 82, pp. 102615, 2021.
- [16] Qi Chen, Xiaoxi Chen, Haorui Song, Zhiwei Xiong, Alan Yuille, Chen Wei, and Zongwei Zhou, "Towards generalizable tumor synthesis," in *Proceedings of the IEEE/CVF Conference on Computer Vision and Pattern Recognition*, 2024, pp. 11147–11158.
- [17] Linshan Wu, Jiaxin Zhuang, Xuefeng Ni, and Hao Chen, "Freetumor: Advance tumor segmentation via large-scale tumor synthesis," *arXiv preprint arXiv:2406.01264*, 2024.
- [18] Yao Zhang, Nanjun He, Jiawei Yang, Yuexiang Li, Dong Wei, Yawen Huang, et al., "mmformer: Multimodal medical transformer for incomplete multimodal learning of brain tumor segmentation," in *International Conference on Medical Image Computing and Computer-Assisted Intervention*. Springer, 2022, pp. 107–117.
- [19] Yuhang Ding, Xin Yu, and Yi Yang, "Rfnet: Region-aware fusion network for incomplete multi-modal brain tumor segmentation," in *Proceedings of the IEEE/CVF international conference on computer vision*, 2021, pp. 3975–3984.
- [20] Yutian Zhong, Shuangyang Zhang, Zhenyang Liu, Xiaoming Zhang, Zongxin Mo, Yizhe Zhang, Haoyu Hu, Wufan Chen, and Li Qi, "Unsupervised fusion of misaligned pat and mri images via mutually reinforcing cross-modality image generation and registration," *IEEE Transactions on Medical Imaging*, 2023.
- [21] Huafeng Li, Dayong Su, Qing Cai, and Yafei Zhang, "Bsafusion: A bidirectional stepwise feature alignment network for unaligned medical image fusion," *arXiv preprint arXiv:2412.08050*, 2024.
- [22] Virginia Fernandez, Walter Hugo Lopez Pinaya, Pedro Borges, Petru-Daniel Tudosiu, Mark S Graham, Tom Vercauteren, and M Jorge Cardoso, "Can segmentation models be trained with fully synthetically generated data?," in *International Workshop on Simulation and Synthesis in Medical Imaging*. Springer, 2022, pp. 79–90.
- [23] Lingting Zhu, Zeyue Xue, Zhenchao Jin, Xian Liu, Jingzhen He, Ziwei Liu, and Lequan Yu, "Make-a-volume: Leveraging latent diffusion models for cross-modality 3d brain mri synthesis," in *International Conference on Medical Image Computing and Computer-Assisted Intervention*. Springer, 2023, pp. 592–601.
- [24] Zolnamar Dorjsembe, Hsing-Kuo Pao, Sodtavilan Odonchimed, and Furen Xiao, "Conditional diffusion models for semantic 3d brain mri synthesis," *IEEE Journal of Biomedical and Health Informatics*, 2024.
- [25] Ahmad B Qasim, Ivan Ezhov, Suprosanna Shit, Oliver Schoppe, Johannes C Paetzold, Anjany Sekuboyina, et al., "Red-gan: Attacking class imbalance via conditioned generation. yet another medical imaging perspective.," in *Medical imaging with deep learning*. PMLR, 2020, pp. 655–668.
- [26] Pengxiao Xu, Junyan Lyu, Li Lin, Pujin Cheng, and Xiaoying Tang, "Lf-synthseg: Label-free brain tissue-assisted tumor synthesis and segmentation," *IEEE Journal of Biomedical and Health Informatics*, 2024.
- [27] Li Lin, Linkai Peng, Huaqing He, Pujin Cheng, Jiewei Wu, Kenneth KY Wong, and Xiaoying Tang, "Yolocurvseg: You only label one noisy

- skeleton for vessel-style curvilinear structure segmentation,” *Medical Image Analysis*, vol. 90, pp. 102937, 2023.
- [28] Roman Suvorov, Elizaveta Logacheva, Anton Mashikhin, Anastasia Remizova, Arsenii Ashukha, Aleksei Silvestrov, et al., “Resolution-robust large mask inpainting with fourier convolutions,” *Winter Conference on Applications of Computer Vision (WACV)*, pp. 3172–3182, 2021.
- [29] Robin Rombach, Andreas Blattmann, Dominik Lorenz, Patrick Esser, and Björn Ommer, “High-resolution image synthesis with latent diffusion models,” in *Proceedings of the IEEE/CVF conference on computer vision and pattern recognition*, 2022, pp. 10684–10695.
- [30] Patrick Bilic, Patrick Christ, Hongwei Bran Li, Eugene Vorontsov, Avi Ben-Cohen, Georgios Kaissis, et al., “The liver tumor segmentation benchmark (lits),” *Medical Image Analysis*, vol. 84, pp. 102680, 2023.
- [31] Fausto Milletari, Nassir Navab, and Seyed-Ahmad Ahmadi, “V-net: Fully convolutional neural networks for volumetric medical image segmentation,” *Fourth International Conference on 3D Vision*, pp. 565–571, 2016.
- [32] Ozan Oktay, Jo Schlemper, Loic Le Folgoc, Matthew Lee, Mattias Heinrich, Kazunari Misawa, et al., “Attention u-net: Learning where to look for the pancreas,” *ArXiv*, vol. abs/1804.03999, 2018.
- [33] Ali Hatamizadeh, Vishwesh Nath, Yucheng Tang, Dong Yang, Holger R Roth, and Daguang Xu, “Swin unetr: Swin transformers for semantic segmentation of brain tumors in mri images,” in *International MICCAI brainlesion workshop*. Springer, 2021, pp. 272–284.
- [34] Andriy Myronenko, “3d mri brain tumor segmentation using autoencoder regularization,” in *BrainLes@MICCAI*, 2018.
- [35] Taesung Park, Alexei A Efros, Richard Zhang, and Jun-Yan Zhu, “Contrastive learning for unpaired image-to-image translation,” in *Computer Vision—ECCV 2020*. Springer, 2020, pp. 319–345.